Structural and Optical Constants of Annealed $As_{47.5}Se_{47.5}Ag_5$ Film using DSC Transformation Curve

E.R. Shaaban[a,*], M.A. Abdel-Rahim[b], M.N. Abd-el Salam[b,c], Mansour Mohamed[b], A.Y. Abdel-Latief[b] and El Sayed Yousef[d,e]

[a]Physics Department, Faculty of Science A1-Azhar University, Assiut 71542, Egypt
[b]Physics Department, Faculty of Science, Assiut University, Assiut 71516, Egypt
[c]High Institute for Engineering and Technology, El-Minya 61768, Egypt
[d]Physics Dep., Faculty of Science, King Khalid University, P.O. Box 9004, Abha, Saudi Arabia
[e]Research Center for Advanced Materials Science (RCAMS), King Khalid University, Abha 61413, P.O. Box 9004, Saudi Arabia

(Received April 27, 2018; in final form September 11, 2018)

The effect of thermal annealing process on both structural and optical properties of amorphous $As_{47.5}Se_{47.5}Ag_5$ thin films was studied. The X-ray diffraction studies exhibit that the crystallinity was improved by increasing the annealing temperature. Further, the crystallite size and the crystallinity increase whereas dislocation density and strain decrease with increase of annealing temperatures. The optical constants of the as-prepared and annealed of $As_{47.5}Se_{47.5}Ag_5$ thin films were calculated using envelope method. The optical absorption data in these films were successfully describes by Tauc's relation which exhibit the indirect transitions for as-prepared sample and allowed direct transition for annealed sample above onset temperature T_c. It is evident that the energy gap E_g^{opt} decreases and the localized states E_e increases as a function annealing temperature. The dispersion of the refractive index n for these films was discussed using the single oscillator model proposed by the Wemple–DiDomenico relationship.

DOI: 10.12693/APhysPolA.135.401

PACS/topics: $As_{47.5}Se_{47.5}Ag_5$ thin films, annealing temperatures, XRD, optical properties, single oscillator parameters

1. Introduction

Chalcogenide glasses are formed from group VI elements (S, Se, and Te) of the periodic table. Glassy alloys containing chalcogen elements were initially studied for their interesting semiconducting properties and more recent applications in reversible phase-change optical recording, memory switching and optical data storage [1, 2]. Thermal annealing is an important method for investigation of the reduction of the intrinsic defects in amorphous state and study the transition from amorphous state to crystalline state of the same materials for using switching electrical and optical devices [1–6].

Furthermore, the amorphous-crystalline semiconductors materials based on Se, Te, and S have a high third order non-linearity and are often alloyed with Ge, Sb, or As in order that obtain higher sensitivity and crystallization temperature as well as ageing effects, so in order to beat these problems the As, Se, and As_2Se_3 are considered among the most studied binary systems [7–9]. Otherwise, addition Ag atom on chalcogenide glasses exhibit a peculiar characteristic of mixed ionic-electronic conductors, which provide dynamical ion movement by electron excitation.

Also, lead to develop the glass forming area and create compositional and configurational disorder in the system and has large effect on their structural, physical and thermal properties, thus are considered as candidate materials in batteries, optics, optoelectronics, chemistry, and biology [3, 10–16]. Generally, the non-linear refractive index of chalcogenide glasses of Ag-doped is higher than that of the un-doped glasses because the presence of silver (transition-metal) atoms formed easily polarizable electron clouds is a evident advantage [14]. Optical properties of the Ag doped As–Se chalcogenide thick films have been determined with high precision for optoelectronics applications have been reported our previous work [3].

In the present work, the effect of thermal annealing process on both the structural and optical properties of amorphous $As_{47.5}Se_{47.5}Ag_5$ chalcogenide thin film was investigated. X-ray diffraction pattern has been carried out to follow the structural changes resulting from heat treatment of the as-prepared films at different temperatures. Also, the effect of structural transformations on their optical properties was also investigated.

2. Experimental procedures

2.1. Preparation of the bulk material

Bulk sample of As–Se–Ag was prepared using melt quenching technique from mixing of As, Se, and Ag elements with purity 99.999% (Aldrich ChemCo, USA). Ac-

*corresponding author; e-mail: esam_ramadan2008@yahoo.com

cording to their atomic percentage the stoichiometric ratios were shut-in a quartz glass ampoule under a vacuum of 10^{-5} Torr. Through the heating process the ampoule must be frequently rocked to ensure the homogeneity of molten materials. After achieving the desired time, the ampoule containing the molten materials were rapidly quenched in a mixture of ice and water to get the bulk glass of As–Se–Ag [17]. The crystallization kinetics of $As_{47.5}Se_{47.5}Ag_5$ glass was investigated using a Shimadzu 50 differential scanning calorimeter (DSC) with an accuracy of ±0.1 K. More details are shown in Ref. [17].

2.2. Preparation of the thin films

Thin films of As–Se–Ag sample were prepared by thermal evaporation technique using a coating unit (DV-502A; Denton Vacuum, Cherry Hill, NJ, USA) under high vacuum conditions (10^{-7} mbar). The substrates utilized for deposition were carefully cleaned using ultrasonic hot bath distilled water and pure alcohol before the evaporation process started [3]. The structure and phase of the as-deposited films and annealed films in a vacuum of (10^{-3} Torr) with five different temperatures 463, 532, 604, 613, and 623 K, respectively, for a fixed time (30 min) and then cooled down to room temperature. The annealed thin films were examined using a Philips 1710 X-ray diffractometer (XRD). The transmittance and reflectance spectra for as-deposited and annealed films were obtained by a double-beam computer-controlled spectrophotometer (UV-2101, Shimadzu) at normal light incidence in the range of wavelength from 400 to 2500 nm.

3. Results and discussion

3.1. Structural characterization

The DSC curves for the as-prepared $As_{47.5}Se_{47.5}Ag_5$ glass at heating rate 20 K/min shown in Fig. 1. One can have observed three characteristic phenomena are clear in the temperature range. Only one glass transition temperatures T_g, onset crystallization temperature T_c and the peaks of crystallization T_p. The thermal annealing applied to the sample of $As_{47.5}Se_{47.5}Ag_5$ thin films at five various annealed temperatures 463, 532, 604, 613, and 623 K, respectively, with a heating rate of 20 K/min at a fixed time (30 min) under nitrogen gases in the range of glass transition temperature and maximum crystallization temperature of composition under studied (see Fig. 1). The thickness of the annealed samples were calculated in terms of envelop method, it was 1383 nm (for more details see Ref. [3]). XRD was used to monitoring the transformation from amorphous to gradually crystalline thin films as shown in Fig. 2. One can see the films annealed at 532 K are typically still in amorphous state.

The increase of the annealing temperatures till the onset temperature (at 604 K) leads to that the film starts to convert from amorphous state to crystalline state. The

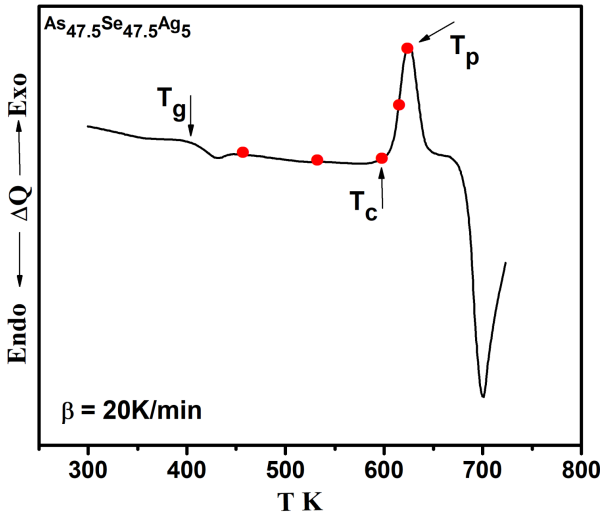

Fig. 1. The DSC traces curve of $As_{47.5}Se_{47.5}Ag_5$ at heating rate of 20 K/min.

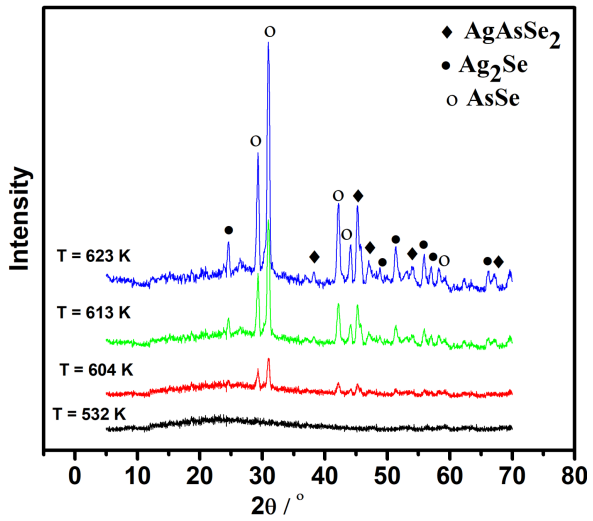

Fig. 2. X-ray diffraction patterns of $As_{47.5}Se_{47.5}Ag_5$ thin films for annealed different temperatures.

sharpness of the intensity of the peaks increase with increase of the annealing temperature. This means that the thermal annealing leads to the rearrangement atoms and eliminates the crystal defects in the film. The X-ray diffraction patterns of the annealed films show a presence of AsSe, $AgAsSe_2$, and Ag_2Se phases. The main crystalline phase is AsSe with (M: monoclinic) crystal structure with a unit cell defined by $a = 0.669$ nm, $b = 0.1386$ nm and $c = 1$ nm according to the ICDS [card no. (00-037-1122)] [18]. Another two crystalline phases of $AgAsSe_2$ (T: tetragonal) and Ag_2Se (O: orthorhombic) appear with increase of the annealing temperature according to cards numbers [card no. (00-033-1165)], [card no. (01-071-2410)], respectively, [19, 20]. Table I shows the comparative interplanar spaces for both typically (d_{exp}) and standard (d_{stand}) cards for all phases that appear with increase of the annealing temperatures.

TABLE I

The X-ray structure data, phases observed, crystallite size D, dislocation density δ and strain ε of different annealing temperatures for $As_{47.5}Se_{47.5}Ag_5$ thin films. (M: monoclinic, T: tetragonal, O: orthorhombic)

Annealing temp. [K]	$d_{exp.}$ [Å]	d_{stand} [Å]	Phases	*hkl* plane	Crystallite size D [nm]	Strain , $\varepsilon \times 10^{-4}$	Dislocation density, $\delta \times 10^{14}$ [m^{-2}]
604	3.04	3.05	AsSe	(-141) M	67.17	0.10	2.22
	2.89	2.89	AsSe	(122) M	61.1	0.104	2.67
	2.14	2.14	AsSe	(212) M	56.78	8.43	3.10
	2.00	1.99	$AgAsSe_2$	(225) T	45.49	9.74	4.83
613	3.05	3.05	AsSe	(-141) M	86.8	7.77	1.33
	2.89	2.89	AsSe	(122) M	93.43	6.84	1.15
	2.14	2.14	AsSe	(212) M	61	7.76	2.69
	2.05	2.06	AsSe	(152) M	61.4	7.39	2.65
	2.00	1.99	$AgAsSe_2$	(225) T	79.8	5.55	1.57
	1.93	1.93	$AgAsSe_2$	(315) T	66.8	6.39	2.24
	1.39	1.39	$AgAsSe_2$	(606) T	72.22	4.26	1.92
	3.62	3.63	Ag_2Se	(110) O	69.8	0.115	2.05
	1.77	1.77	Ag_2Se	(104) O	55.6	7.07	3.24
	1.64	1.66	Ag_2Se	(222) O	46.6	7.81	4.61
623	3.05	3.05	AsSe	(-141) M	75.26	8.45	1.76
	2.89	2.89	AsSe	(122) M	79.47	5.71	1.58
	2.14	2.14	AsSe	(212) M	97.14	4.87	1.06
	2.05	2.06	AsSe	(152) M	79.49	5.71	1.58
	1.58	1.58	AsSe	(262) M	90.12	3.88	1.23
	2.35	2.35	$AgAsSe_2$	(224) T	68.77	7.56	2.11
	2.00	1.99	$AgAsSe_2$	(225) T	130.94	3.38	5.83
	1.93	1.93	$AgAsSe_2$	(315) T	54.64	7.81	3.35
	1.69	1.69	$AgAsSe_2$	(552) T	56.23	6.67	3.16
	1.39	1.39	$AgAsSe_2$	(606) T	58.92	5.29	2.88
	3.62	3.63	Ag_2Se	(110) O	69.81	0.115	2.05
	1.86	1.87	Ag_2Se	(014) O	73.86	5.59	1.84
	1.77	1.77	Ag_2Se	(104) O	60.66	6.48	2.72
	1.64	1.66	Ag_2Se	(222) O	85.23	4.26	1.38
	1.61	1.61	Ag_2Se	(213) O	80.39	2.38	1.55

In terms of XRD pattern, the crystallite size D, dislocation density δ, and the micro-strain ε can be calculated as a function of annealing temperature, which plays an important role in several properties such as thermal stability and mechanical properties. The average crystallite size D of all crystalline phases was calculated according to Scherrer's equation [21]:

$$D = \frac{K\lambda}{\beta \cos\theta}, \tag{1}$$

where K is a shape factor known as the Scherrer constant normally equal to 0.94 and β is the full width at half maximum (FWHM) of the peak. The dislocation density "δ" (i.e. the dislocation lines per unit area) of the crystal can be calculated once the crystallite size "d" is estimated using the formula [22]:

$$\delta = \frac{1}{D^2}. \tag{2}$$

On the other hand, the origin of the strain is also related to the lattice mismatch and may be calculated from the following relation [23]:

$$\varepsilon = \left(\frac{\lambda}{D\cos\theta} - \beta\right)\frac{1}{\tan\theta}. \tag{3}$$

The calculated values of D, δ and ε are listed in Table I. The values of the crystallite size are increased whereas the dislocation density and strain are decreased with increase of the annealing temperatures. This may be due to attributed to the decreasing in lattice defects among the grain boundaries [24, 25]. The dependence of the average crystallite size D, dislocation density δ, and lattice strain ε, of the main AsSe phase formed as a function of annealing temperatures are shown in Fig. 3.

3.2. Absorption coefficient and optical band gap analysis

Figure 4 shows the variation of absolute spectral values of reflectance R and transmittance T versus wavelength λ for both deposited and annealed of $As_{47.5}Se_{47.5}Ag_5$ thin film. One can notice that the transmittance increases with increase of the annealing temperature and the absorption edge shifted towards higher wavelength due to changes in the structural properties of the films owing to the increase of annealing temperature. The absorption

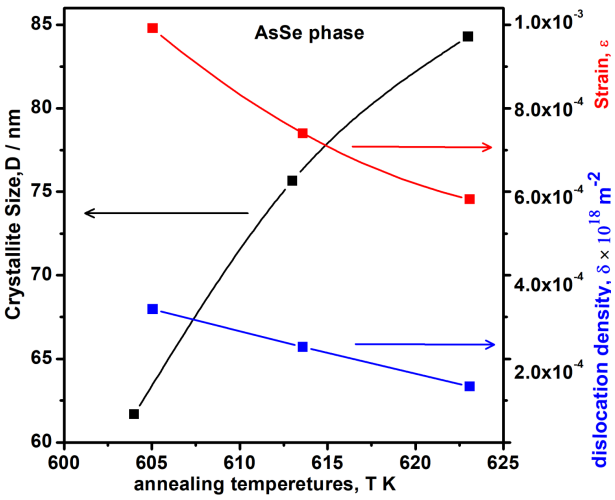

Fig. 3. The thermal processes dependence of the crystallite size D, dislocation density δ and strain ε of AsSe phase formed in $As_{47.5}Se_{47.5}Ag_5$ thin films.

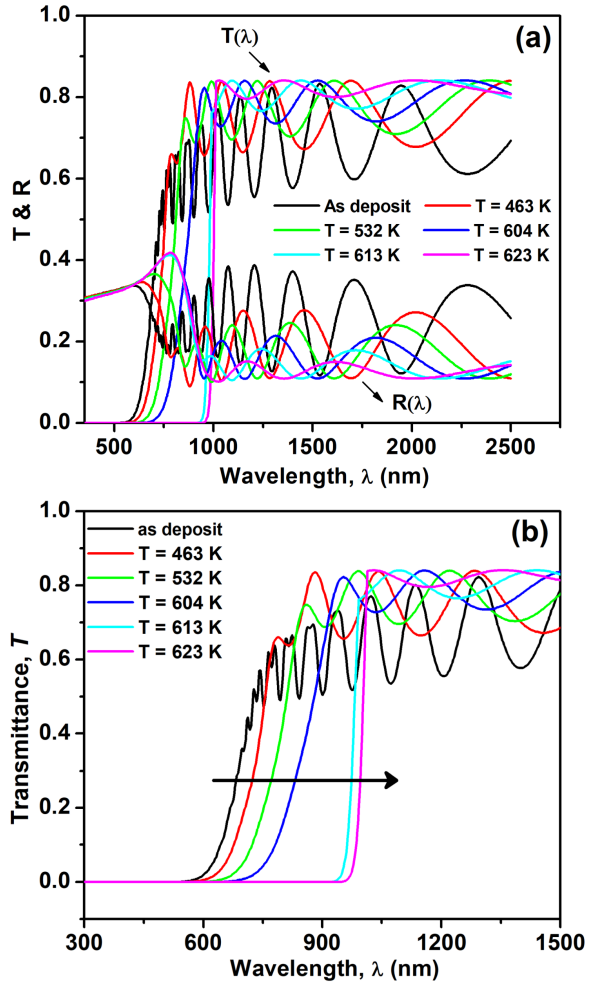

Fig. 4. (a) The optical transmittance T_λ and reflectance R_λ spectrum of as prepared and different annealing temperatures for $As_{47.5}Se_{47.5}Ag_5$ thin films. (b) The red shift of transmission spectra in strong absorption region of as prepared and different annealing temperatures for $As_{47.5}Se_{47.5}Ag_5$ thin films.

coefficient α can be calculated in strong absorption region using both transmission T and reflection R spectra [26]:

$$\alpha = \frac{1}{d} \ln \left(\frac{(1-R)^2 + \sqrt{(1-R)^4 + 4(TR)^2}}{2T} \right), \qquad (4)$$

where d is the thickness of the films that can be determined by Swanepoel's method (mentioned below). Figure 5 shows the variation values of the absorption coefficient α versus photon energy $h\upsilon$ as a function of annealing temperature for $As_{47.5}Se_{47.5}Ag_5$ thin film. The absorption edge shifts towards the lower photon energies. It is clear that the absorption edge ($\alpha \geq 10^4$) shifts towards the lower photon energy with increase of the annealing temperature that is related to the decrease of the optical band gap.

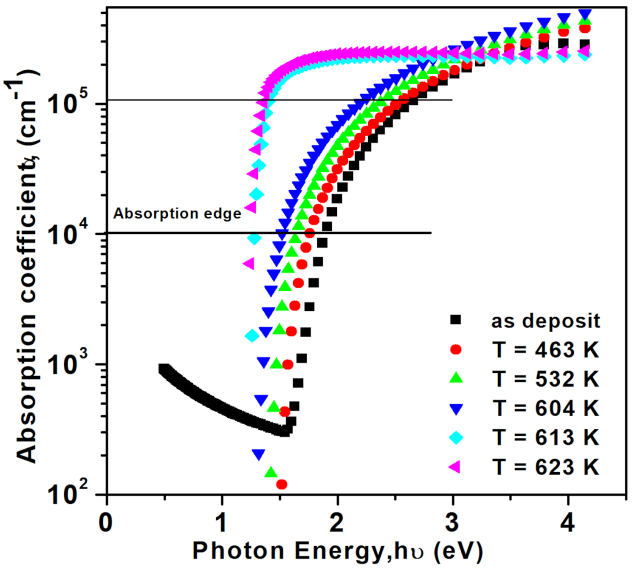

Fig. 5. The variation of the absorption coefficient α with the photon energy $h\upsilon$ of as prepared and annealed different temperatures for $As_{47.5}Se_{47.5}Ag_5$ thin films.

According to the Tauc relation at the end of absorption edge region ($\alpha \geq 10^4$ cm^{-1}) [27] the optical energy band gap E_g can be calculated using the values of the absorption coefficient α:

$$\alpha(h\upsilon) = \frac{B(h\nu - E_g)^r}{h\nu}, \qquad (5)$$

where B is a constant parameter dependent on the transition probability and $r = 1/2$ for direct transition band gap and $r = 2$ for non-direct transition band gap. For all different annealing temperatures (463, 532, and 604 K) of $As_{47.5}Se_{47.5}Ag_5$ thin films the indirect transitions are valid and the direct transitions are valid.

In this study the direct transition is valid for annealed $As_{47.5}Se_{47.5}Ag_5$ thin films after the inset of crystallization temperatures at 613 and 623 K. For all different annealing temperatures of $As_{47.5}Se_{47.5}Ag_5$ thin films the indirect transitions and the direct transitions are valid. Figure 6 shows the $(\alpha h\nu)^{1/2}$ vs. $h\nu$ for as-deposited and annealing temperatures 463, 532 and 604 K while the

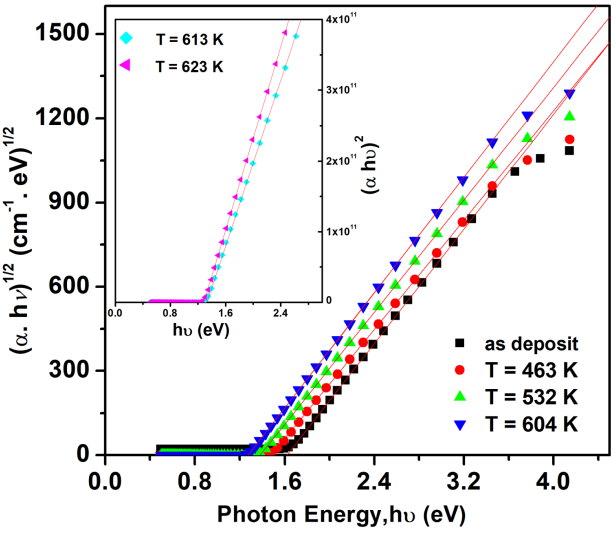

Fig. 6. The plots of indirect transitions and direct transitions with the photon energy $h\upsilon$ of as prepared and annealed different temperatures for $As_{47.5}Se_{47.5}Ag_5$ thin films.

$(\alpha h\nu)^2$ vs. $h\nu$ for annealing temperatures 613 and 623 K. The optical energy band gap E_g of the films was evaluated from the intercept of linear portion of each curve for different annealing temperature with the $h\nu$ in the abscissa, i.e. at $(\alpha h\nu)^{1/2} = 0$, $(\alpha h\nu)^2 = 0$, respectively, see in Fig. 6. The annealing process conformed the crystallinity of the films. Furthermore, the increase of the annealing temperature may increase the crystallite size. Therefore, the decrease in the energy band gap may be attributed to quantum confinement phenomena.

Moreover, the absorption coefficient at less than about $\alpha \approx 10^4$ cm^{-1} near the absorption edge depends exponentially on $h\upsilon$ as [28]:

$$\alpha(h\upsilon) = \alpha_0 \exp \frac{h\upsilon}{E_e}, \tag{6}$$

where α_o is a constant, E_e is the Urbach energy and is determined from plotting ln α vs. $h\upsilon$ as shown in Fig. 7. The deduced values of the band gap, E_g and E_e (obtained from the slope of the straight lines of Fig. 7), are listed in Table II. It is evident from the results that the values of E_g decrease with increase of annealed temperature while the Urbach energy E_e increases with increase of annealed temperature. This may be as a result to the increase of the lattice parameter and hence the unit cell size, also the amorphous-crystalline transformations after annealing are responsible for decrease of the film optical gap [5, 25, 29].

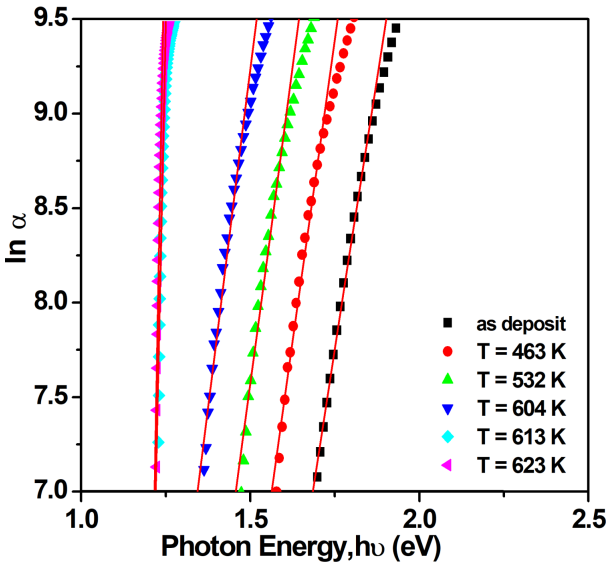

Fig. 7. ln α versus $h\upsilon$ for $As_{47.5}Se_{47.5}Ag_5$ thin films at annealed different temperatures.

TABLE II

Values of the Cauchy coefficient parameters (A, B), energy gap $E_g^{\rm opt}$, width of localized states E_e and dispersion parameters of annealing temperatures 463, 532, 604, 613, and 623 K for $As_{47.5}Se_{47.5}Ag_5$ thin film.

Annealing temperature [K]	Cauchy coefficient		$E_g^{\rm opt}$ [eV]	E_e [eV]	E_d [eV]	E_o [eV]	n_o	ε_o	ε_l	$s_o \times 10^{13}$ [m^2]	λ_o [nm]
	A	$B \times 10^5$									
as-deposit	2.296	5.003	1.612	0.089	10.712	3.175	2.091	4.372	11.7	2.37	478.7
463	2.267	3.924	1.491	0.095	11.628	3.191	2.155	4.644	10.1	2.27	465.8
532	2.16	3.806	1.387	0.102	12.443	2.982	2.274	5.171	9.2	2.09	458.8
604	2.143	1.957	1.274	0.108	13.387	2.772	2.414	5.827	8.3	2.02	438.2
613	1.965	2.582	1.344	0.092	14.603	2.541	2.597	6.744	7.5	1.76	430.9
623	1.852	2.456	1.348	0.090	14.455	2.567	2.575	6.631	7.04	1.48	424.5

3.3. Refractive index and dispersion parameters

The refractive index n of the annealing films under study can be calculated according to envelope method using transmission spectrum proposed by Swanepoel [30, 31]. Figure 8 illustrates the transmittance spectrum for annealing temperature 463 K. As example using this method the same procedure was applied to the other different annealing temperatures. The refractive index n can be deduced at any wavelength using the formula

$$n = \sqrt{N + (N^2 - s^2)^{1/2}}, \tag{7}$$

where

$$N = 2s\frac{T_M - T_m}{T_M T_m} + \frac{s^2+1}{2},$$

$$s = \frac{1}{T_s} + \left(\frac{1}{T_s^2}\right)^{1/2}. \quad (8)$$

T_M and T_m are the transmittance maximum and minimum, respectively, at a certain wavelength. The procedure adopted to deduce the refractive index n of as-prepared thin films, see our previous published work [3].

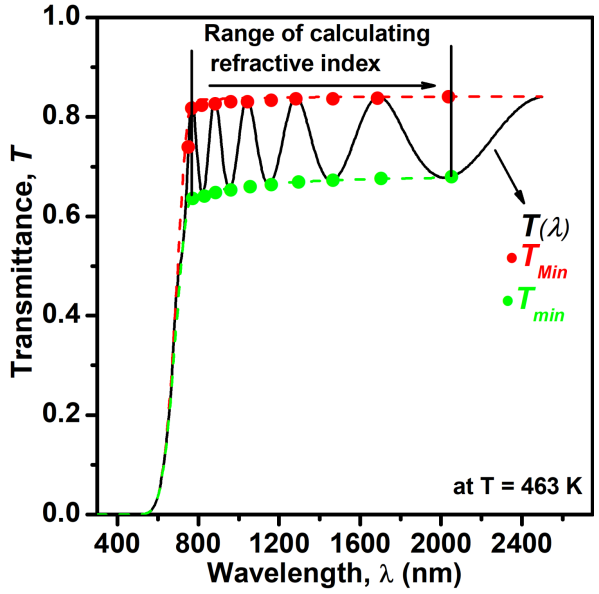

Fig. 8. The optical transmittance T_λ at annealed temperatures 463 K for $As_{47.5}Se_{47.5}Ag_5$ thin films.

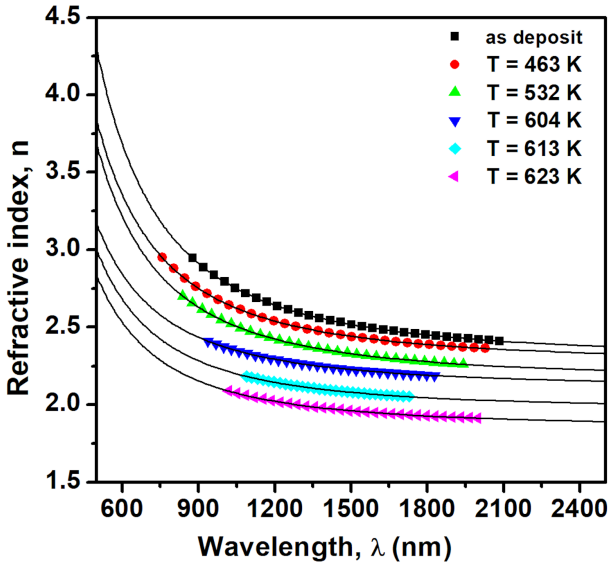

Fig. 9. The variation of refractive index n with wavelength λ for $As_{47.5}Se_{47.5}Ag_5$ thin films at annealed different temperatures.

The dependence of refractive index n with wavelength for all annealing temperatures thin films under studied are evident in Fig. 9. In the strong absorption spectral region, the values of the refractive index n can be fitted using the two-term Cauchy dispersion relationship, $n(\lambda) = a + b/\lambda^2$, which can be used for extrapolating the complete overall wavelengths [32] (see solid lines in Fig. 9). Figure 9 shows that with increase of the annealing temperature the refractive index n decreases. This behavior may be attributed to the reduction of the number of unsaturated defects, which causes the reduction in the density of localized states in the band structure consequently decreasing the refractive index [33]. The values of Cauchy coefficient A and B are clear in Table II. Furthermore, the values of extinction coefficient k can be calculated from the absorption coefficient α and wavelength λ values using the formula $k = \alpha\lambda/4\pi$. Figure 10 shows the extinction coefficient versus the wavelength for $As_{47.5}Se_{47.5}Ag_5$ thin film at different temperature of annealing. It is clearly seen that the extinction coefficient increases with increase of the annealing temperature.

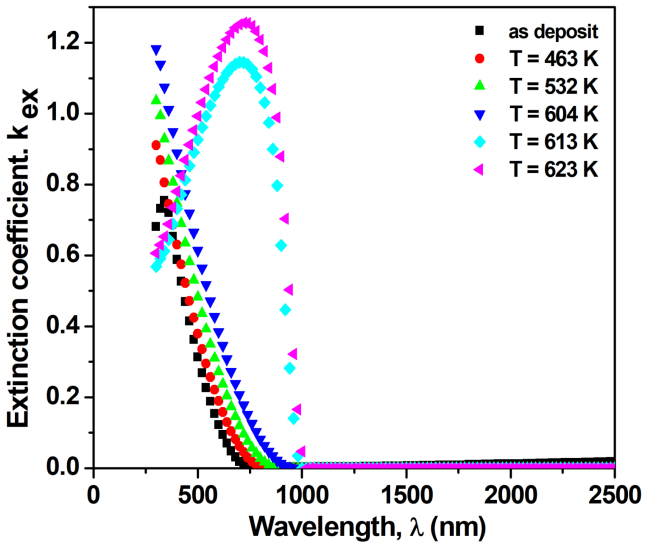

Fig. 10. Plots of the extinction coefficient, k versus $h\nu$ for $As_{47.5}Se_{47.5}Ag_5$ thin films at various annealed temperatures.

Now, the values of dispersion refractive index for $As_{47.5}Se_{47.5}Ag_5$ thin films at different annealing temperature can be analyzed according to the single-oscillator model suggested by the Wemple–DiDomenico (WDD) by the relation [16]:

$$n^2 = 1 + \left(\frac{E_o E_d}{E_o^2 - (h\nu)^2}\right), \quad (9)$$

where E_o is the single-oscillator energy and E_d is the dispersion energy. The plot of $(n^2-1)^{-1}$ vs. $(h\nu)^2$ is shown in Fig. 11. The values of E_o and E_d are determined from the intercept E_o/E_d and the slope $(E_o E_d)^{-1}$ of the straight lines. Further, it is obviously found that E_o de-

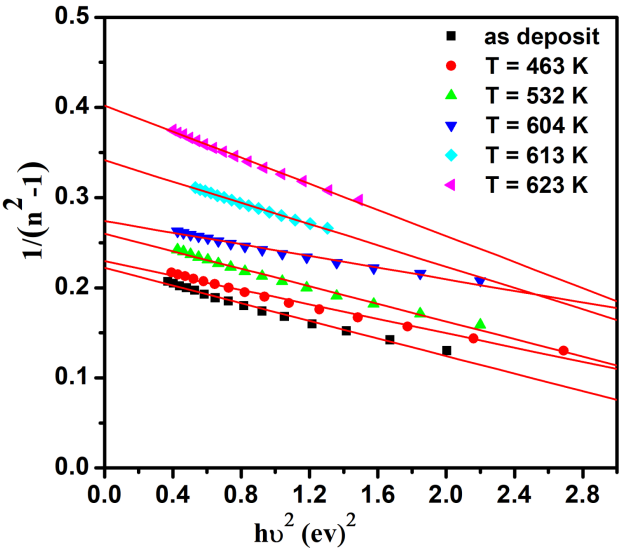

Fig. 11. Plots of $1/(n^2\text{-}1)$ versus $h\upsilon$ for $As_{47.5}Se_{47.5}Ag_5$ thin films at various annealed temperatures.

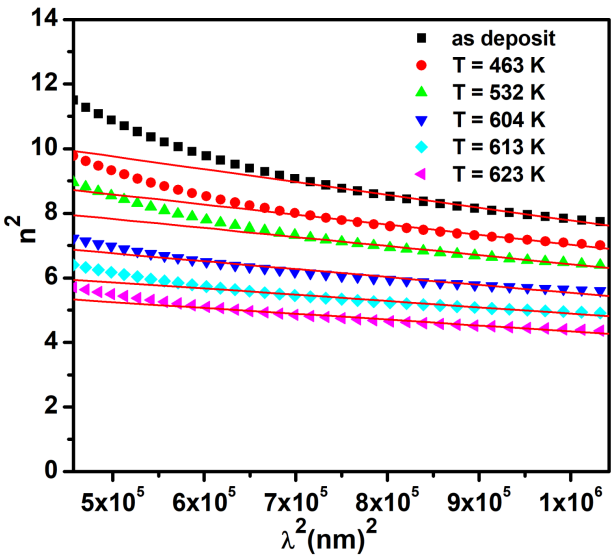

Fig. 12. Plots of n^2 versus λ^2 for $As_{47.5}Se_{47.5}Ag_5$ thin films at various annealed temperatures.

creases, while E_d increases with increase of the thermal annealed temperature as shown in Table II. The decrease of E_o values reveals that the strength of the inter-band optical transitions decreases with increase of the thermal process. But the increase of the E_d values with the annealed temperatures maybe attributed to the increase of the rate of diffusion of atoms in the films which gives more number of atoms at interstitial sites, this lead to impurity type scattering centers [34].

In order that deduce the high frequency dielectric constant (ε_l) we have further analyzed the data of refractive index dependence photon's energy $h\upsilon$ through two procedures, the first is proceeding the relation between the lattice high frequency dielectric constant (ε_l) and the refractive index, n that is given by the following relation [16]:

$$n^2 = \varepsilon_l - \frac{e^2 N \lambda^2}{4\pi c^2 \varepsilon_o m^*}, \tag{10}$$

where e is electron charge, N is the number of free carriers to the effective mass m^*. Figure 12 shows the plots of n^2 vs. λ^2 for the different annealing temperatures. The values of ε_l were determined from the intercept with the ordinate $\lambda^2 = 0$ and given in Table II.

Additionally, the static refractive index n_o for all annealing temperatures was determined using the subsequent relation

$$n_o = (1 + E_d/E_o)^{1/2}. \tag{11}$$

Thus the values of zero-frequency dielectric constant $\varepsilon_o = n_o^2$ were deduced. The values of the n_o and ε_o for all the annealing temperatures for all films are listed in Table II. The values of n_o and ε_o increase with the increase of the thermal process and $\varepsilon_o < \varepsilon_l$. This behavior may be owing to the contribution of charge in the polarization process that occurs inside the material when the light is incident on it [25].

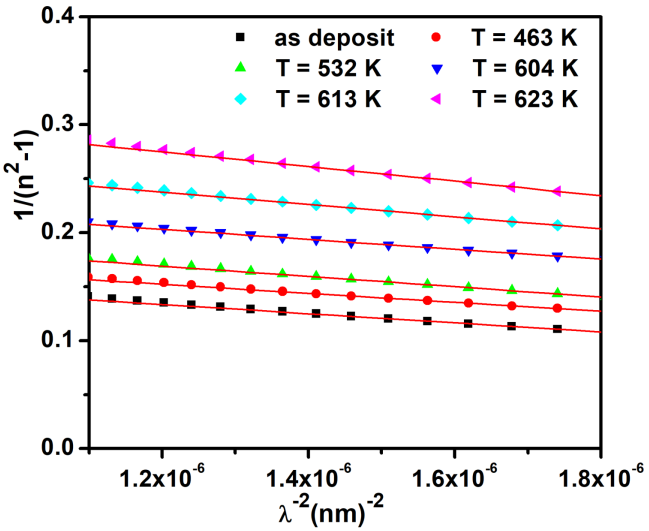

Fig. 13. Plots of $1/(n^2\text{-}1)$ versus λ^{-2} for $As_{47.5}Se_{47.5}Ag_5$ thin films at various annealed temperatures.

The second proceeding to deduce the inter-band oscillator wavelength (λ_o) and the oscillator strength (s_o) for $As_{47.5}Se_{47.5}Ag_5$ thin films at different annealing temperatures by using the single Sellmeier oscillator [35]:

$$\frac{n_\infty^2 - 1}{n^2 - 1} = 1 - \left(\frac{\lambda_o}{\lambda}\right)^2. \tag{12}$$

The values of λ_o and s_o for all annealing temperatures films were calculated from the slope and intercept of the plots of $(n^2\text{-}1)^{-1}$ vs. λ^{-2} (see in Fig. 13) and were given in Table II. The values of parameters λ_o and s_o change with change of the annealing temperatures. These changes show that the film is suitable to change of refractive index and oscillator parameters by changing annealing temperature [16, 36].

4. Conclusions

X-ray diffraction has been used to examine the structures of the as-deposited and annealed $As_{47.5}Se_{47.5}Ag_5$ thin films. Swanepoel's method has been introduced to find the film thickness, refractive index, and hence other optical constants. The results of XRD demonstrate that the crystallinity of the main phase AsSe is improved by increase of the annealing temperature in the range of crystallization area of DSC curve. Furthermore, the dislocation density and lattice strain decrease with increase of annealing temperatures. The optical band gaps of $As_{47.5}Se_{47.5}Ag_5$ thin films at different annealing temperature can be determined in the strong absorption region and satisfied indirect transition for amorphous thin film and direct transition for annealed crystalline thin film. The optical band gap decreases with increase of the annealing temperature. The decrease in the energy band gap E_g may be attributed to quantum confinement phenomena. Also, the refractive index decreases with increase of the annealing temperature. This behavior may be attributed to the reduction of the number of unsaturated defects, which causes the reduction in the density of localized states in the band structure. Finally, the dispersion parameters such as E_d, E_o, ε_o, ε_l, s_o and λ_o are sensitive to thermal processes.

Acknowledgments

The authors are grateful to Assiut University and Al-Azhar University (Assiut branch) for supporting with experimental measurements and the authors also thank the Deanship of Scientific Research at King Khalid University (KKU) for funding this research project, Number: (RCAMS/KKU/001-18) under Research Center for Advanced Material Science.

References

[1] A. Zakery, S.R. Elliott, *J. Non-Cryst. Solids* **330**, 1 (2003).

[2] V. Shiryaev, C. Boussard-Plédel, P. Houizot, T. Jouan, J.-L. Adam, J. Lucas, *Mater. Sci. Eng. B* **127**, 138 (2006).

[3] E.R. Shaaban, M.N. Abd-el Salam, M. Mohamed, M.A. Abdel-Rahim, A.Y. Abdel-Latief, *J. Mater. Sci. Mater. Electron.* **28**, 13379 (2017).

[4] J. Singh, *Optical Properties of Condensed Matter and Applications*, Wiley, 2006.

[5] E. Shaaban, H. Elshaikh, M. Soraya, *Optoelectron. Adv. Mater. Rapid Commun.* **9**, 587 (2015).

[6] V. Takats, A.C. Miller, H. Jain, A. Kovalskiy, S. Kokenyesi, *Thin Solid Films* **519**, 3437 (2011).

[7] T. Petkova, P. Petkov, S. Vassilev, Y. Nedeva, *Surf. Interface Anal.* **36**, 880 (2004).

[8] K. Mietzsch, A.G. Fitzgerald, *Appl. Surf. Sci.* **162-163**, 464 (2000).

[9] J. Harbold, F. Ilday, F. Wise, J. Sanghera, V. Nguyen, L. Shaw, I. Aggarwal, *Opt. Lett.* **27**, 119 (2002).

[10] M. Frumar, T. Wagner, *Curr. Opin. Solid State Mater. Sci.* **7**, 117 (2003).

[11] W. Shen, S. Baccaro, A. Cemmi, J. Ren, Z. Zhang, Y. Zhou, Y. Yang, G. Chen, *Nucl. Instrum. Methods Phys. Res. B* **329**, 48 (2014).

[12] M.I. Abd-Elrahman, A.Y. Abdel-Latief, R.M. Khafagy, N. Younis, M.M. Hafiz, *Spectrochim. Acta A* **137**, 29 (2015).

[13] K. Tanaka, *Thin Solid Films* **66**, 271 (1980).

[14] K. Ogusu, J. Yamasaki, S. Maeda, M. Kitao, M. Minakata, *Opt. Lett.* **29**, 265 (2004).

[15] E.R. Shaaban, *Philos. Mag.* **88**, 781 (2008).

[16] S.H. Wemple, M. DiDomenico Jr., *Phys. Rev. B* **3**, 1338 (1971).

[17] M. Mohamed, M.N. Abd-el Salam, M.A. Abdel-Rahim, A.Y. Abdel-Latief, E.R. Shaaban, *J. Thermal Anal. Calorim.* **132**, 91 (2017).

[18] M. Kotkata, A. Shamah, M. El-Den, M. El-Mously, *Acta Phys. Hung.* **54**, 49 (1983).

[19] Y.E.A. Voroshilov, *Sov. Phys. Crystallogr.* **21**, 333 (1976).

[20] G.A. Wiegers, *Am. Mineralogist* **56**, 1882 (1971).

[21] P. Scherrer, *Nachr. Ges. Wiss. Goettingen Math. Phys.* **K1**, 98 (1918).

[22] M. Dhanam, R. Balasundaraprabhu, S. Jayakumar, P. Gopalakrishnan, M. Kannan, *Phys. Status Solidi A* **191**, 149 (2002).

[23] S. Venkatachalam, D. Mangalaraj, S.K. Narayandass, *Physica B Condens. Matter* **393**, 47 (2007).

[24] E.R. Shaaban, I. Kansal, S. Mohamed, J.M. Ferreira, *Physica B Condens. Matter* **404**, 3571 (2009).

[25] M. El-Hagary, M. Emam-Ismail, E. Shaaban, A. Al-Rashidi, S. Althoyaib, *Mater. Chem. Phys.* **132**, 581 (2012).

[26] R. Vahalová, L. Tichý, M. Vlček, H. Tichá, *Phys. Status Solidi A* **181**, 199 (2000).

[27] J. Tauc, *Amorphous and Liquid Semiconductor*, Plenum, New York 1974, Ch. 4, p. 159.

[28] R. Urbach, *Phys. Rev.* **92**, 1324 (1953).

[29] A.H. Moharram, *Appl. Surf. Sci.* **143**, 39 (1999).

[30] R. Swanepoel, *J. Phys. E Sci. Instrum.* **17**, 896 (1984).

[31] R. Swanepoel, *J. Phys. E Sci. Instrum.* **16**, 1214 (1983).

[32] T.S. Moss, *Optical Properties of Semiconductors*, Butterworth, London 1959.

[33] S.A. Khan, J.K. Lal, A.A. Al-Ghamdi, *Opt. Laser Technol.* **42**, 839 (2010).

[34] M.A. Abdel-Rahim, M.M. Hafiz, A.Z. Mahmoud, *Solid State Sci.* **48**, 125 (2015).

[35] A. Walton, T. Moss, *Proc. Phys. Soc.* **81**, 509 (1963).

[36] H.M. Kotb, M. Dabban, A. Abdel-Latif, M. Hafiz, *J. Alloys Comp.* **512**, 115 (2012).